An update to this article is included at the end

Biophysical Chemistry 326 (2025) 107503

Contents lists available at ScienceDirect

Biophysical Chemistry

journal homepage: www.elsevier.com/locate/biophyschem

Effect of disialoganglioside GD3 on the subgel, gel and fluid phases of cationic DODAB vesicles

Julia B. Ejarque [a,1], Anna C.F. Couto [a,1,2], Thábata Matos [a], Evandro L. Duarte [b], M. Teresa Lamy [b], Julio H.K. Rozenfeld [a,*]

[a] Departamento de Biofísica, Escola Paulista de Medicina, Universidade Federal de São Paulo, R. Botucatu 862, 04023-062 São Paulo, SP, Brazil
[b] Instituto de Física, Universidade de São Paulo, Rua do Matão 1371, 05508090 São Paulo, SP, Brazil

ARTICLE INFO

Keywords:
GD3 ganglioside
Dioctadecyldimethylammonium bromide
Differential scanning calorimetry
electron paramagnetic resonance
Subgel

ABSTRACT

GD3 is a disialoganglioside overexpressed in several types of cancer cells. The synthetic cationic lipid DODAB has been successfully employed as a vaccine adjuvant, and would be suitable to enhance GD3 immunogenicity. Here, mixed dispersions of GD3 and DODAB were characterized by Differential Scanning Calorimetry (DSC) and Electron Paramagnetic Resonance (EPR) spectroscopy. GD3 is miscible with DODAB, and decreases the DODAB gel-fluid transition cooperativity. GD3 does not affect the temperature hysteresis between gel-fluid and fluid-gel transitions. GD3 does not affect the formation of a subgel phase in DODAB bilayers cooled below 15 °C. GD3 decreases the acyl chain packing of the DODAB subgel phase, which could explain the broad and shallow exothermic event between 5 °C and 20 °C that appears on thermograms of mixed dispersions. These results might contribute to the development of novel GD3-based cancer immunotherapies, including at the low temperatures involved in cold chain stability.

1. Introduction

Gangliosides are glycosphingolipids that contain at least one sialic acid in their oligosaccharide headgroup [1]. They are involved in several physiological processes, such as cell adhesion, signal transduction and apoptosis [1,2], as well as in pathological processes such as inflammation, cancer and neurodegenerative disorders [1–4].

The pathophysiological roles of gangliosides derive from their ability to form membrane domains [5], and the major brain gangliosides, GM1, GD1a, GD1b and GT1b have been comprehensively investigated [5–7].

Albeit less studied, the disialoganglioside GD3 (Fig. 1) is also a very interesting subject: it is the most abundant ganglioside in the human colostrum [8], and it is important for early neurological development in mice due to its abundance in neural stem cells [9]. GD3 is involved in the control of apoptosis [10], being overexpressed in several aggressive forms of cancer, such as melanoma, glioblastoma and neuroblastoma [4]. It was also shown to induce immune responses by NKT cells [11,12], what makes it a potential target for cancer immunotherapy [13].

The cationic lipid dioctadecyldimethylammonium bromide (DODAB) is a versatile carrier for nucleic acids [14], hydrophobic drugs [15], and antigens [16,17]. It has also been successfully employed as a vaccine adjuvant [18], because it induces potent humoral and cellular immune responses [16]. Hence, DODAB could be a suitable carrier for GD3 vis-a-vis developing new cancer immunotherapies.

Despite the intensive biophysical characterization of gangliosides [5,19], no study has been made on mixtures of gangliosides and cationic lipids so far. In the present work, Differential Scanning Calorimetry (DSC) and Electron Paramagnetic Resonance (EPR) spectroscopy are used to characterize mixed dispersions of cationic DODAB and anionic GD3. These techniques have been chosen because DSC gives information about the thermotropic behavior of lipids [20], and EPR spectroscopy gives information about order and mobility of lipid dispersion carriers at different depths [21,22]. In fact, EPR spectroscopy has been extensively used to characterize DODAB dispersions [23].

* Corresponding author.
E-mail address: julio.rozenfeld@unifesp.br (J.H.K. Rozenfeld).
[1] These authors contributed equally to this work
[2] Present address: Instituto de Química, Universidade Estadual de Campinas, 270 Monteiro Lobato, Campinas, SP, 13083–862, Brazil.

https://doi.org/10.1016/j.bpc.2025.107503
Received 23 May 2025; Received in revised form 28 July 2025; Accepted 31 July 2025
Available online 4 August 2025
0301-4622/© 2025 Elsevier B.V. All rights are reserved, including those for text and data mining, AI training, and similar technologies.

2. Experimental methods

2.1. Materials

Dioctadecyldimethylammonium bromide (DODAB, Lot # BCBR1922V), and HEPES buffer were purchased from Sigma Chemical Co. (St. Louis, MO, USA). GD3 from bovine milk (Lot # 860060–01-010), and paramagnetic probes 1-palmitoyl-2-stearoyl-(*n*-doxyl)-sn-glycero-3-phosphocholine (*n*-PCSL, $n = 5$ or 16) were purchased from Avanti Polar Lipids (Birmingham, AL, USA).

The chemical structures of lipids and spin labels are shown in Fig. 1.

2.2. Preparation of lipid dispersions

Chloroform/methanol 2:1 (*v*/v) solutions containing DODAB, GD3, or DODAB and GD3, were dried under a nitrogen stream and left under reduced pressure for 2 h. The resulting lipid films were then dispersed in HEPES buffer (10 mM, pH 7.4) by heating for 20 min at 87 °C in a water bath. Heating was accompanied by vortexing at every 5 min in order to ensure a homogeneous dispersion.

For EPR experiments, 0.8 mol% of 5-PCSL or 0.3 mol% of 16-PCSL were added to the chloroform/methanol solutions prior to lipid film formation. The lipid films were dispersed as described above. Final DODAB concentration was 2 mM. Final GD3 concentration was 0.1 mM, which corresponds to 4.8 mol% of the total lipid concentration.

2.3. Differential scanning calorimetry (DSC)

DSC thermograms were obtained in a Microcal VP-DSC Microcalorimeter (Microcal Inc., Northampton, MA, USA). Heating and cooling rates were 20 °C/h. Scans were performed with at least two samples prepared in different days. A heating (annealing) scan of 90 °C/h was performed prior to all experiments. Thermodynamic parameters such as the phase transition temperature (Tm), the phase transition enthalpy (ΔH), and the width at half-maximum ($\Delta T_{1/2}$) were obtained from analyses using the Microcal Origin software. Tm is the temperature at the maximum value of heat capacity (ΔCp) [24]. ΔH values are obtained by integrating the area under the thermograms. $\Delta T_{1/2}$ is the temperature range (width) at half peak height, and was obtained from the most intense peaks, either the gel-fluid or the fluid-gel transitions.

2.4. Electron paramagnetic resonance (EPR) spectroscopy

A Bruker EMX spectrometer equipped with the ER4119HS high sensitivity cavity was used to obtain EPR spectra in the X band. The microwave power was 13.4 mW, the modulation frequency was 100 kHz, and the modulation amplitude was 1 G. Sample temperatures were kept within 0.1 °C using a Bruker BVT-2000 variable temperature device.

The values of maximum (Amax) and minimum (Amin) hyperfine splittings and those of the low (h_{+1}), central (h_0) and high (h_{-1}) field line amplitudes were measured directly from the spectra (see Figs. 3 and 5).

The effective order parameter, S_{eff}, was calculated from the expression [25].

$$S_{eff} = \frac{A_{\parallel} - A_{\perp}}{A_{zz} - (1/2)(A_{xx} + A_{yy})} \frac{a'_o}{a_o}$$

where $a'_o = (1/3)(A_{xx} + A_{yy} + A_{zz})$, $a_o = (1/3)(A_{\parallel} + 2A_{\perp})$, $A_{//}$ (= A_{max}) is the maximum hyperfine splitting directly measured in the spectrum (see Fig. 5), $A_{\perp} = A\left[1 - \frac{A_{//} - A_{min}}{A_{zz} - (1/2)(A_{xx} + A_{yy})}[]\right]_{min}$, A_{min} is the measured inner hyperfine splitting (see Fig. 5) and A_{xx}, A_{yy} and A_{zz} are the principal values of the hyperfine tensor for doxylpropane [26].

Each experiment was performed at least in duplicate with samples prepared on different occasions, and standard deviations are shown as error bars.

3. Results

3.1. GD3 affects the DODAB gel-fluid transition profile, but not the transition hysteresis

The heating and cooling thermograms of DODAB and DODAB + GD3 dispersions are shown in Fig. 2.

When heated, 2 mM DODAB dispersions have a sharp endothermic peak at 46.9 °C (Fig. 2), corresponding to the main gel-fluid phase transition of unilamellar vesicles [27,28]. A smaller, broader

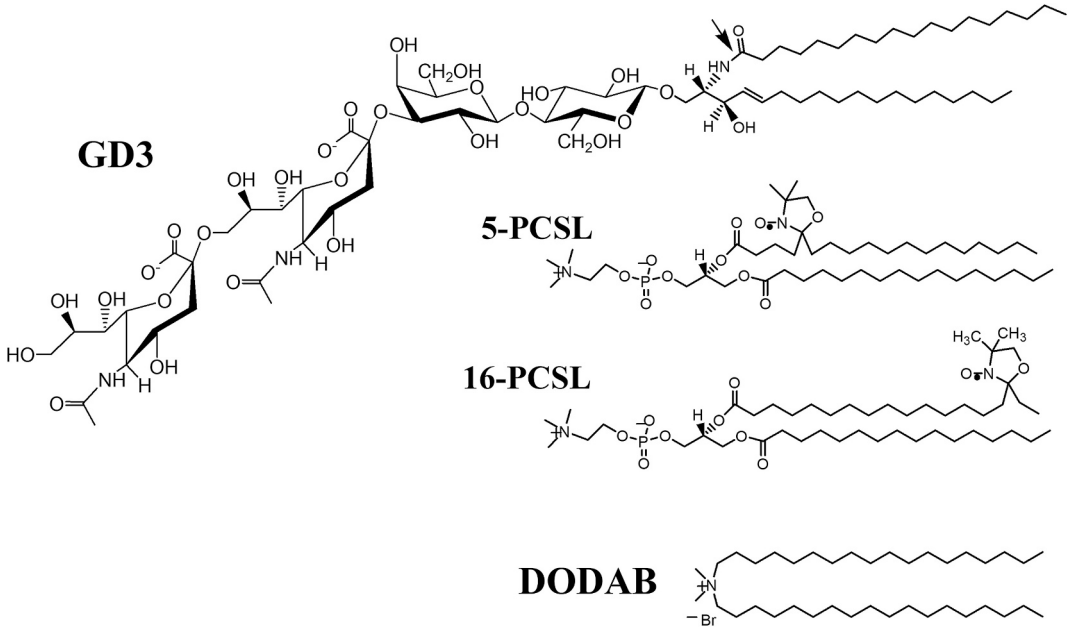

Fig. 1. Chemical structures of GD3, 5-PCSL, 16-PCSL and DODAB. The arrow indicates the amide bond connecting the acyl chain to the sphingosine of the GD3 ceramide.

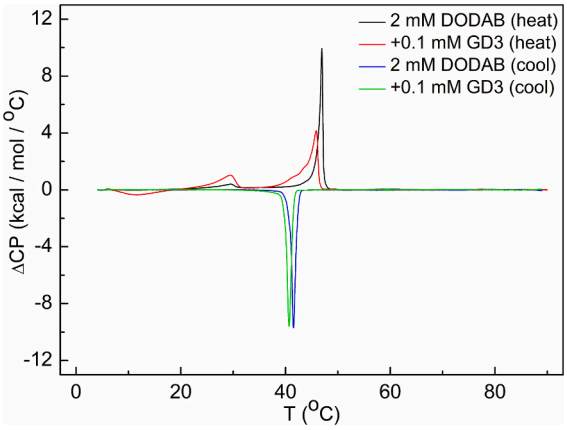

Fig. 2. Effect of 0.1 mM GD3 on the DSC thermograms of 2 mM DODAB vesicles. Scan rates for heating and cooling were 20 °C/h.

endothermic peak is also observed at 29.9 °C, which corresponds to the subgel – gel transition observed for samples incubated below 15 °C [29,30]. In the cooling scan, a single sharp exothermic peak is observed at 41.4 °C, corresponding to the fluid-gel transition. The temperatures for all the transitions observed in Fig. 2 are different from those described for dispersions prepared in pure water [29–31], possibly because the HEPES buffer is able to partially shield the electrostatic repulsion between cationic DODAB headgroups. Accordingly, a gel-fluid transition at 46.9 °C and a fluid-gel transition at 41.5 °C have been previously described for samples prepared in HEPES [27,32].

Mixed dispersions of 2 mM DODAB and 0.1 mM GD3 have a broader, less intense endothermic peak at 45.8 °C in the heating scan (Fig. 2), corresponding to the mixed bilayer gel-fluid transition. The endothermic subgel-gel peak is observed at 29.3 °C, and it is more intense than the one observed for pure DODAB vesicles (Fig. 2). A broad exothermic event spanning the 5 °C to 20 °C range and peaking at 12 °C is also observed in the heating scan (Fig. 2). This event will be discussed in the next Sections. However it is noteworthy that a very similar heating thermogram profile is observed for dispersions of 2 mM DODAB and 0.05 mM GD3 (Supplementary Fig. S1).

When the mixed DODAB + GD3 dispersions are cooled, a single sharp exothermic peak corresponding to the fluid-gel transition is observed at 40.6 °C (Fig. 2).

Table 1 summarizes the thermodynamic parameters obtained from the thermograms shown in Fig. 2. These parameters are the transition temperature (Tm), the transition enthalpy (ΔH), and the width (temperature range) at half-maximum peak ($\Delta T_{1/2}$). Tm is the temperature at the highest ΔCp value [24]. ΔH is obtained by integrating the curves and represent the enthalpy changes per molecule of lipid [24]. $\Delta T_{1/2}$ is a measure of phase transition cooperativity: if a transition is less cooperative, it takes a larger $\Delta T_{1/2}$ value to be completed [24,33]. In order to facilitate the discussion of the thermal events observed in the thermograms (Fig. 2), the analyses were performed in separate temperature ranges.

In the temperature range of 5 °C to 20 °C, a single exothermic event is observed in the heating scan of DODAB + GD3 mixtures (Fig. 2). This event peaks at 12 °C and has the smallest ΔH value of all events listed in Table 1. It is also the least cooperative event, displaying the highest $\Delta T_{1/2}$ value (Table 1).

In the temperature range of 20 °C to 35 °C, the subgel-gel pre-transition peak at 29.9 °C for heating scans of pure DODAB vesicles is within the range of experimental error of the 29.3 °C peak that is observed in presence of GD3 (Table 1). GD3 does not affect the cooperativity of the pre-transition, with a $\Delta T_{1/2}$ value of about 4 °C. However, the ΔH value increases in presence of GD3 (Table 1). Hence, GD3 increases the energy necessary to complete the subgel-gel pre-transition.

In the temperature range of 35 °C to 90 °C, data from the heating scans show that the gel-fluid Tm is decreased by 1 °C in presence of GD3 (Table 1). The transition cooperativity is significantly decreased in presence of GD3, since the $\Delta T_{1/2}$ value more than doubles. The ΔH value is decreased within the experimental error range in presence of GD3 (Table 1). Hence, although GD3 affects the gel-fluid cooperativity, it does not affect the transition energy.

From the cooling scans, it is possible to observe that GD3 does not affect the ΔH value of the fluid-gel transition, which remains at about −11 kcal/mol (Table 1). The $\Delta T_{1/2}$ value is increased to 1.3 °C, but within the experimental error range (Table 1), implying that no change of cooperativity is observed for the fluid-gel transition in presence of GD3. Similarly to what is observed in the heating scans of the 35 °C to 90 °C range, the fluid-gel Tm is also decreased by 1 °C in presence of GD3 (Table 1).

In Fig. 2, it is possible to observe that the gel-fluid and fluid-gel transitions do not occur at the same temperature. This temperature hysteresis can be quantified from the difference in Tm values of heating and cooling shown in Table 1. For pure DODAB vesicles, this hysteresis is of 5.5 °C. Since GD3 decreases by 1 °C both Tm values of heating and cooling at the 35 °C to 90 °C range (Table 1), the hysteresis is not changed when GD3 is mixed with DODAB.

3.2. *Below the gel-fluid transition temperature, GD3 increases the superficial rigidity but decreases the packing of the DODAB bilayers core*

The structures of pure DODAB and mixed DODAB + GD3 aggregates were compared using the paramagnetic probes 5-PCLS and 16-PCSL, which give information about microviscosity and packing near the interface and the core of lipid bilayers, respectively [23]. Fig. 3 shows the spectra of these probes embedded in pure 2 mM DODAB and mixed 2 mM DODAB +0.1 mM GD3 dispersions below the gel-fluid transition temperature.

The spectra of 5-PCSL and 16-PCSL embedded in pure DODAB vesicles are very different at all temperatures shown in Fig. 3. The spectra of 5-PCSL are characteristic of a more anisotropic microenvironment, in which the movement of the probe is more restricted due to increased

Table 1
Thermodynamic parameters of 2 mM DODAB and 2 mM DODAB +0.1 mM GD3 dispersions.

	Temperature range			Temperature range			Temperature range		
	5–20 °C			20–35 °C			35–90 °C		
Dispersion	T_m (°C)	ΔH (kcal/mol)	$\Delta T_{1/2}$ (°C)	T_m (°C)	ΔH (kcal/mol)	$\Delta T_{1/2}$ (°C)	T_m (°C)	ΔH (kcal/mol)	$\Delta T_{1/2}$ (°C)
	Heating cycle								
DODAB	–	–	–	29.9 ± 0.3	3.4 ± 0.9	4 ± 1	46.9 ± 0.1	14 ± 2	0.7 ± 0.1
+ GD3	12 ± 1	−2.4 ± 0.2	7 ± 1	29.3 ± 0.3	5.2 ± 0.6	4.1 ± 0.1	45.8 ± 0.1	12.5 ± 0.3	1.7 ± 0.1
	Cooling cycle								
DODAB	–	–	–	–	–	–	41.4 ± 0.1	−11.7 ± 0.7	0.8 ± 0.1
+ GD3	–	–	–	–	–	–	40.6 ± 0.1	−11.3 ± 0.4	1.3 ± 0.6

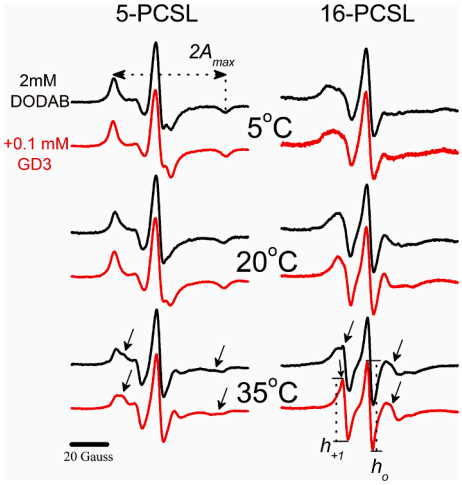

Fig. 3. EPR spectra of 5-PCSL and 16-PCSL embedded in 2 mM DODAB vesicles, with or without 0.1 mM GD3, at temperatures below the gel-fluid transition. The maximum hyperfine splitting (Amax) and the amplitudes of low (h + 1) and central (h0) field lines are indicated. The total spectra width is 100 G. Arrows indicate the features of a more isotropic component which coexists with the typical gel phase signal at 35 °C.

molecular packing. In comparison, the spectra of 16-PCSL are typical of a more isotropic microenvironment, where the probe has a higher mobility, and lower order, due to a decreased molecular packing (Fig. 3).

This gradient of increasing flexibility from the surface to the core of the bilayer is typical of non-interdigitated lamellar structures [26], and has been extensively described for DODAB bilayers in the gel phase [23,34]. This flexibility gradient is not affected by the presence of GD3 (Fig. 3), indicating that GD3 does not induce bilayer interdigitation.

At 5 °C and 20 °C, the spectra display features of a single EPR signal (Fig. 3). These spectra are similar in presence or absence of GD3 (Fig. 3). On the other hand, at 35 °C, more isotropic features are present, and indicate that a less rigid population coexists with the typical DODAB gel phase (Fig. 3). The coexistence of two phases has been described for pure DODAB vesicles at temperatures around Tm [35]. This coexistence of phases is also observed in presence of GD3 (Fig. 3).

Up to 30 °C, the spectra of both probes display features of a single EPR signal (Fig. 3, Supplementary Fig. S2). Hence, some empirical parameters that can be obtained from the spectra can be used to compare the structures of these aggregates [23].

For instance, the maximum hyperfine splitting (Amax) can be directly obtained from the spectra of 5-PCSL (Fig. 3). It is a useful parameter because it is sensitive to the packing and viscosity of the probe microenvironment: decreasing of packing or viscosity results in smaller Amax values [23]. In the 16-PCSL spectra the Amax values cannot be accurately determined because of increased isotropy (Fig. 3). Therefore, information about the structure around this probe can be obtained from the ratio of the low and central field line amplitudes (h + 1/h0) (Fig. 3). The values of this ratio increase as the bilayers become less packed [23].

Fig. 4 shows the values of Amax and h + 1/h0 for DODAB and DODAB + GD3 dispersions at temperatures below the gel-fluid transition.

The increase in temperature results in a decrease in molecular packing, so the Amax values for both dispersions decrease with increasing temperature (Fig. 4A). However, Amax values are higher for dispersions of DODAB + GD3 at all temperatures tested, indicating that GD3 increases the superficial packing of DODAB bilayers (Fig. 4A).

The decrease in molecular packing caused by temperature increase is also observed by the increase in h + 1/h0 values for both dispersions (Fig. 4B). The increase in h + 1/h0 values is higher for the DODAB +

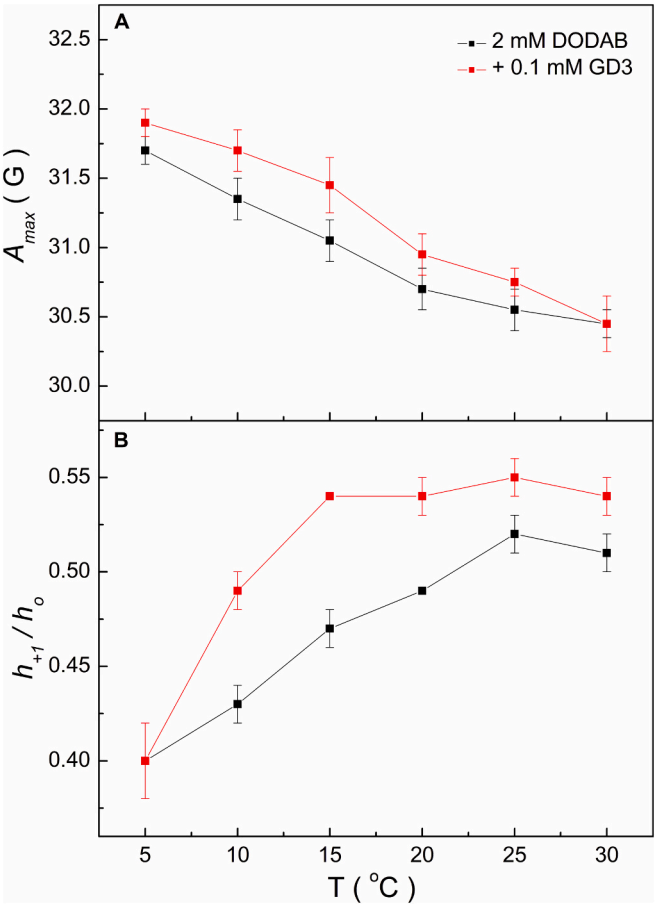

Fig. 4. Effect of 0.1 mM GD3 on the maximum hyperfine splitting (Amax) of 5-PCSL (A) and on the ratio of the low and central field line amplitudes (h + 1/h0) of 16-PCSL (B) embedded in 2 mM DODAB vesicles at temperatures below the gel-fluid transition. Error bars indicate standard deviations.

GD3 dispersions, showing that GD3 decreases the molecular packing of the DODAB bilayers' core (Fig. 4B). Hence, GD3 has different effects on the molecular packing near the surface and core of DODAB bilayers at temperatures below the gel-fluid transition.

3.3. Above the gel-fluid transition temperature, GD3 increases the molecular packing both near the surface and at the core of DODAB bilayers

Fig. 5 shows the spectra of 5-PCSL and 16-PCSL embedded in pure DODAB and mixed DODAB + GD3 dispersions above the gel-fluid transition temperature.

The spectra of 5-PCSL shown in Fig. 5 have thinner features when compared to the ones at the lower temperatures shown in Fig. 3. These thinner features indicate that the probes have fast movement along their long axis [26], which is typical of a fluid yet microscopically ordered structure close to the bilayer interface.

The spectra of 16-PCSL display sharp peaks (Fig. 5), indicating a fast and nearly isotropic movement of the nitroxide label, which is typical of the fast motional regime observed in fluid bilayers [26].

Again, the spectra of both paramagnetic probes are similar in DODAB and DODAB + GD3 dispersions at all temperatures tested, and the empirical parameters can be more useful for the structural analysis.

As shown in Fig. 5, the maximum and minimum hyperfine splittings (Amax and Amin) can be accurately measured in the 5-PCSL spectra. These hyperfine splittings are used to calculate the effective order parameter (Seff, see Section 2.4), which gives information about the acyl

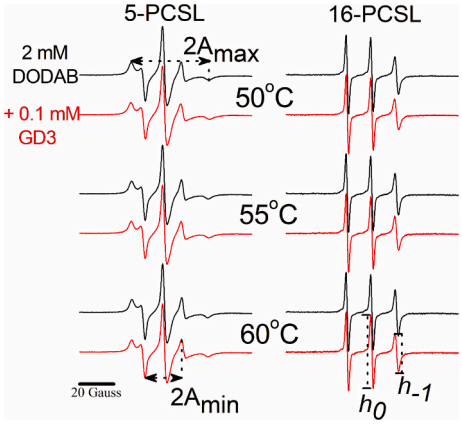

Fig. 5. Effect of 0.1 mM GD3 on the EPR spectra of 5-PCSL and 16-PCSL embedded in 2 mM DODAB vesicles at temperatures above the gel-fluid transition. The maximum and minimum hyperfine splittings (Amax and Amin), and the amplitudes of central (h0) and high (h-1) field lines are indicated. The total spectra width is 100 G.

chain order [36,37].

The hyperfine splittings are not clearly defined in the 16-PCSL spectra (Fig. 5), which sense a less ordered environment. On the other hand, the amplitudes of the high (h-1) and central (h0) field lines can be accurately measured (Fig. 5), and the ratio of these amplitudes (h-1/h0) can be used to evaluate viscosity and packing in a similar way to the one previously described for the h + 1/h0 ratio in the previous Section: the values of h-1/h0 increase as the bilayer viscosity decreases [23].

Fig. 6 shows the values of Seff and h-1/h0 for DODAB and DODAB + GD3 dispersions at temperatures above the gel-fluid transition.

The Seff values are higher for DODAB + GD3 than for pure DODAB dispersions at all temperatures tested (Fig. 6A), indicating that GD3 increases the superficial order of DODAB bilayers. A similar trend is observed for h-1/h0: their values are smaller for DODAB + GD3 than for pure DODAB dispersions at all temperatures tested (Fig. 6B), indicating that GD3 increases the rigidity of the core of DODAB bilayers. In summary, GD3 increases the molecular packing and ordering of the DODAB bilayers in the fluid phase.

4. Discussion

When dispersed in HEPES 10 mM pH 7.4, DODAB self assembles into vesicles [28,38], while GD3 forms micelles that are able to embed the paramagnetic labels 5-PCSL and 16-PCSL [39]. The spectra of these probes in GD3 micelles show features of a relatively fluid environment in temperatures as low as 5 °C [39].

In the temperature range of 5 °C to 30 °C, these fluid features disappear when GD3 is mixed with DODAB (Fig. 3 and Supplementary Fig. S2), and the mixture of DODAB and GD3 result in EPR spectra of a single signal, indicative of a single population of spin labeled lipids (Fig. 3 and Supplementary Fig. S2). This suggests that DODAB and GD3 are miscible, because if more than one EPR signal was present in these spectra, it would indicate that either GD3 is not embedded in the DODAB bilayers (remaining as micelles), or that it forms domains within the bilayer by lateral phase separation. Similarly, monolayer experiments show that GD3 is miscible with DPPC in a wide range of molar fractions [40].

Since GD3 forms micelles and DODAB forms vesicles, it would be possible to assume that the mixed DODAB + GD3 dispersions could form an intermediary structure such as a bicelle [41,42]. It was shown that EPR spectra of pure DODAB bicelles display two signals corresponding to the coexistence of a gel planar domain and of a highly curved fluid rim domain at temperatures below the gel-fluid transition [23]. This phase coexistence is not observed at temperatures below the gel-fluid

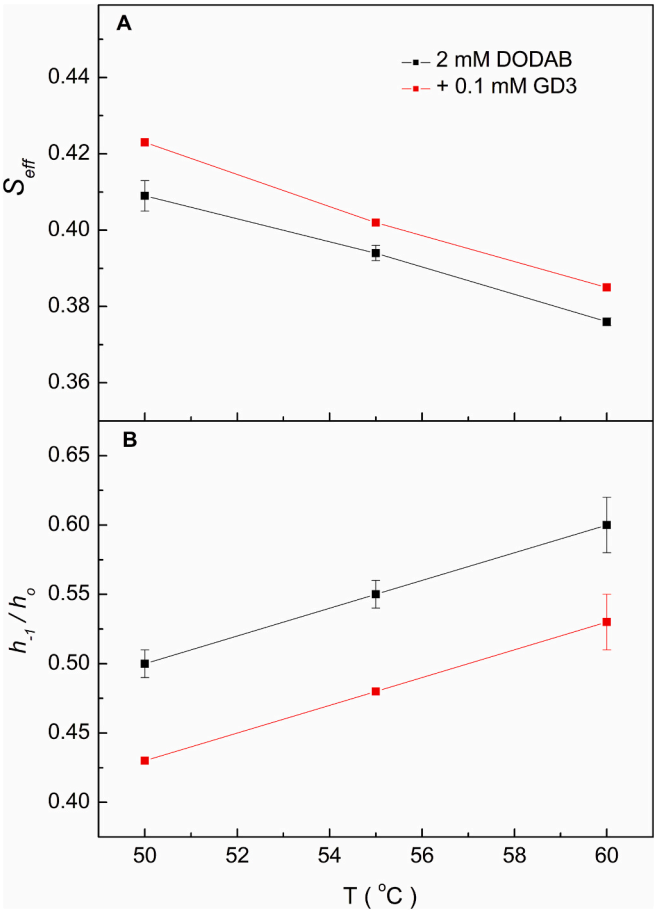

Fig. 6. Effect of 0.1 mM GD3 on the effective order parameter (Seff) of 5-PCSL (A) and on the ratio of the central and high field line amplitudes (h-1/h0) of 16-PCSL (B) embedded in 2 mM DODAB vesicles at temperatures above the gel-fluid transition. Error bars indicate standard deviations.

transition when GD3 is mixed with DODAB (Fig. 3 and Supplementary Fig. S2), suggesting that DODAB and GD3 do not form bicelles.

The appearance and DLS size distributions of the samples with and without GD3 are shown in Supplementary Fig. S3. GD3 does not change the appearance of the DODAB vesicle dispersion and, although a small decrease in the mean hydrodynamic diameter is observed in presence of GD3, the DLS size distribution suggests these polydisperse samples have a global structure of vesicles (Supplementary Fig. S3). If bicelles of DODAB and GD3 were present, a significant decrease in the mean hydrodynamic diameter would be expected [41]. Taken together, the EPR and DLS data suggest that the most likely scenario is that DODAB and GD3 form vesicles, not bicelles.

Pure DODAB vesicles have a thermotropic behavior that is strongly dependent on sample history, such as method of dispersion, lipid concentration, type and concentration of counterions, presence of additives and incubation temperature [28,43]. In the diluted regime of the present work, it is possible to observe two endothermic peaks in the heating scans: the smaller at 29.8 °C corresponds to a subgel-gel transition, and the more intense peak at 46.9 °C corresponds to the main gel-fluid transition (Fig. 2), as previously described [31]. Upon cooling, a single exothermic peak corresponding to the fluid-gel transition is observed at 41.5 °C (Fig. 2).

The temperature hysteresis between the gel-fluid and fluid-gel transitions has been previously described for DODAB dispersions [29,31], and is common in charged lipids [33]. It happens because the transition paths are different upon heating and cooling: near the transition temperature, domains of one phase are present within the matrix

of the other, resulting in strain energy differences [33]. The fact that GD3 does not change the hysteresis (Table 1) suggests that it does not affect the formation of these domains near the transition temperature. Accordingly, the presence of fluid domains within a gel phase matrix is clearly observed at 35 °C for pure and mixed bilayers (Fig. 3).

It is worth noting that 0.1 mM sulfatide (an anionic sulfated galactosylceramide) also did not affect DODAB hysteresis, but higher concentrations, such as 0.2 mM and 0.4 mM, decreased it, possibly by expanding domain areas and reducing strain tension [32,33]. Hence, the effect of glycosphingolipids on DODAB thermal hysteresis might be concentration-dependent.

As mentioned in Section 3.1, GD3 decreases the cooperativity of the DODAB gel-fluid transition in the temperature range of 35 °C to 90 °C (Fig. 2, Table 1). This would be expected for a bulky lipid embedding in the DODAB gel phase, and a similar effect has been observed for mixtures of DODAB with other less complex glycosphingolipids [32,38,44]. However, GD3 does not have the same effect of these lipids in the organization of the surface and core of the gel phase (Fig. 4).

For samples that were not cooled below 20 °C, it was shown that β-glucosylceramide (a precursor to GD3) [44], α-galactosylceramide [34], and sulfatide [32], decrease the rigidity near the surface and the core of DODAB bilayers in the temperature range of 20 °C to 30 °C. However, GD3 increases the rigidity near the surface (Fig. 4A) and decreases the rigidity in the core (Fig. 4B) of DODAB bilayers in the same temperature range.

This decrease in rigidity of the bilayer core could be explained by a V-shape configuration adopted by the ceramide group of GD3 and the other glycosphingolipids: the rigid amide bond connecting the acyl to the sphingosine chains (Fig. 1) adopts a perpendicular orientation towards the axes of these chains that results in a V-shape configuration [45]. This configuration could be further stabilized by the bulky oligosaccharide headgroup of GD3 [46]. The V-shape configuration requires a large lateral area inside the bilayer, resulting in decreased packing of the DODAB gel phase at the bilayer core (Fig. 4B). This suggests that the decrease in gel-fluid cooperativity observed with all these glycosphingolipids is more dependent on hydrophobic chains interactions than on headgroup interactions.

The increase in rigidity near the surface of DODAB bilayers induced by GD3 in the temperature range of 20 °C to 30 °C (Fig. 4A) could be explained by a condensing effect described for other gangliosides such as GM1 [47,48]. Monolayer assays show that GD3 and DPPC can interact with tighter than ideal molecular packing areas, and with polar headgroups in close proximity [40,49]. This condensing effect could also take place with DODAB, which has a smaller headgroup than DPPC [43]. The cationic charge of DODAB could further enhance the condensing effect by favorable dipolar matching of the oppositely charged headgroups [40,49].

The increase in molecular packing and ordering of the DODAB fluid phase both near the surface and the core in presence of GD3 (Fig. 6) could also be explained by the condensing effect and the V-shape configuration. The large lateral area requirement of this configuration would result in less freedom of movement inside the bilayer (Fig. 6B). Accordingly, an increase in fluid phase rigidity has been extensively described for mixtures of gangliosides with fluid phase phospholipids [50–52]. It is important to note that the increase in fluid phase rigidity is not related to formation of domains by lateral phase separation, since a single fluid signal is observed in the EPR spectra of 5-PCSL and 16-PCSL for mixtures of DODAB and GD3 (Fig. 5).

The small endothermic peak at 29.9 °C observed on heating thermograms has been attributed to a subgel-gel transition (Fig. 2). The DODAB subgel phase is formed when DODAB bilayers are cooled below 15 °C [30,31]. The cooling would allow the DODAB molecules to reorganize from a close-to-hexagonal to a more compact close-to-triclinic 2D lattice [30,31]. This reorganization would result in a more tightly packing of the DODAB acyl chains, with a consequent freezing of the individual acyl chains motion and their further stretching [30,31]. The endothermic peak at 29.9 °C appears as a reflex of the energy necessary to complete the order-disorder transition upon subgel heating.

GD3 intensifies the subgel-gel endothermic peak (Fig. 2), even at smaller concentration (Supplementary Fig. S1). The resulting increase in ΔH value (Table 1) could be explained by the increase in superficial packing when GD3 is mixed with the DODAB bilayers in the temperature range of 5 °C to 20 °C, which corresponds to the subgel phase (Fig. 4A). Taken together, the DSC and EPR results suggest that GD3 does not affect the formation of the subgel phase, i.e., it does not interfere with the overall reorganization of the DODAB 2D lattice, but that it does increase the superficial packing of the subgel lattice.

In contrast, GD3 induces a decrease in the molecular packing of the bilayers' core in the temperature range of 5 °C to 20 °C that corresponds to the DODAB subgel phase (Fig. 4B). The reason for this decrease is probably the same as for the decrease observed in the 20 °C to 35 °C range corresponding to the gel phase (Fig. 4B): the V-shaped configuration of GD3 that occupies a large lateral area inside the bilayer. This need for a larger lateral area probably affects more the more tightly packed acyl chains of DODAB in the subgel phase, and might explain why the packing decrease is more intense in the temperature range corresponding to the subgel phase as compared to the range of the gel phase (Fig. 4B).

The decrease in molecular packing of the DODAB bilayers' core induced by GD3 in the temperature range corresponding to the subgel phase (Fig. 4B), might explain the broad exothermic event in the 5 °C to 20 °C range that appears when GD3 is added to the DODAB bilayer (Fig. 2). The fact that this event is also observed at a lower GD3 concentration and at a lower heating scan (Supplementary Fig. S1) indicates that this event depends on DODAB and GD3 mixing, and is not an artifact due to problems in the thermodynamic equilibrium of these mixtures. Moreover, pure GD3 micelles display a single weak and broad endothermic peak around 20 °C upon heating [39]. This endothermic peak probably reflects changes in the surface area occupied by the oligosaccharide headgroup due to water removal or conformational changes [53], and would not explain the exothermic event observed when GD3 is mixed with DODAB (Fig. 2).

A shallow exothermic peak has also been observed for DODAB and DPPC mixtures, where DPPC chains rearrange into a tilted configuration that does not affect the hexagonal lattice of the gel phase [54]. Similarly, it is possible that the V-shape configuration of the GD3 ceramide disrupts the closely packed DODAB subgel acyl chains (Fig. 4B), while the overall triclinic subgel lattice is maintained by superficial condensation with the bulky GD3 headgroup (Fig. 4A). In other words, the broad exothermic event below 20 °C could be attributed to the effect of GD3 hydrophobic chains, while the enhanced endothermic peak characteristic of the subgel-gel transition at 29.9 °C could be attributed to a condensation effect of the bulky and charged GD3 headgroup (Fig. 2). This is in agreement with the idea that different parts of amphiphilic molecules can undergo stepwise changes that reflect regional (head/tail) differences in molecular interactions [55,56].

GD3 is an attractive target for cancer immunotherapy because it is overexpressed in melanoma, glioma, neuroblastoma, and some types of lung cancer, while it has a low and restricted expression in adult extra neural tissues [57]. Although GD3 has been explored in several clinical trials, so far no major impact on patient outcome has been achieved [57]. This might be related to one of the major obstacles in anti-cancer vaccine development: the use of adequate adjuvants, especially those that promote strong cellular responses [58].

DODAB might be an interesting anti-cancer vaccine adjuvant due to its ability to induce the formation of both cellular and humoral responses [16,17]. The present work might contribute to the development of novel GD3-based immunotherapies, and special attention was given to the structure of DODAB and GD3 assemblies at low temperatures, since cold chain stability is an important issue for immunotherapies and vaccines distribution logistics [59].

5. Conclusions

Mixed dispersions of disialoganglioside GD3 and cationic lipid DODAB were characterized by DSC and EPR spectroscopy. EPR spectra show that 4.8 mol% GD3 is miscible with DODAB bilayers. DSC thermograms show that GD3 does not affect the temperature hysteresis between the gel-fluid and fluid-gel transitions of DODAB bilayers. The thermograms also show that GD3 decreases the DODAB gel-fluid transition cooperativity, probably by decreasing gel phase acyl chain packing.

Empirical analysis of EPR spectra shows that GD3 increases the overall rigidity of the DODAB fluid phase and the superficial packing of the gel phase. Although an increase in fluid phase rigidity and a decrease in the gel-fluid transition cooperativity has been described for mixtures of DODAB with other less complex glycosphingolipids, the effect of GD3 on the gel phase superficial organization is very different and is probably due to a condensing effect on the headgroup region. This effect might also contribute to the maintenance of a subgel phase in mixtures of DODAB and GD3 cooled below 15 °C. DSC data show that the subgel-gel transition enthalpy is increased in presence of GD3.

EPR empirical analysis shows that GD3 decreases the acyl chain packing of the DODAB subgel phase, which could explain the broad and shallow exothermic event between 5 °C and 20 °C that appears on thermograms of mixed dispersions.

These results might contribute to the development of more effective GD3-based cancer immunotherapies and vaccines. The characterization of these assemblies at low temperatures might also be important for cold chain logistics stability.

CRediT authorship contribution statement

Julia B. Ejarque: Investigation, Formal analysis. **Anna C.F. Couto:** Investigation. **Thábata Matos:** Visualization. **Evandro L. Duarte:** Methodology, Formal analysis. **M. Teresa Lamy:** Methodology, Formal analysis. **Julio H.K. Rozenfeld:** Writing – original draft, Project administration, Formal analysis, Conceptualization.

Declaration of competing interest

The authors declare the following financial interests/personal relationships which may be considered as potential competing interests.

Julio Henrique Kravcuks Rozenfeld reports financial support was provided by State of Sao Paulo Research Foundation. Julio Henrique Kravcuks Rozenfeld reports financial support was provided by National Council for Scientific and Technological Development. Julio Henrique Kravcuks Rozenfeld reports financial support was provided by Coordination of Higher Education Personnel Improvement. If there are other authors, they declare that they have no known competing financial interests or personal relationships that could have appeared to influence the work reported in this paper.

Acknowledgments

This work was supported by grants #2016/19077-1 and #2016/13368-4, São Paulo Research Foundation (FAPESP). This study was financed in part by the Coordenação de Aperfeiçoamento de Pessoal de Nível Superior - Brasil (CAPES) - Finance Code 001. A.C.F.C. was supported by grant #2019/17207-3, São Paulo Research Foundation (FAPESP). M.T.L. and E.L.D. are part of the National Institute of Science and Technology Complex Fluids (INCT-FCx), financed by CNPq (465259/2014-6) and FAPESP (2014/50983-3).

Data availability

Data will be made available on request.

References

[1] S. Groux-DeGroote, Y. Guérardel, P. Delannoy, Gangliosides: structures, biosynthesis, analysis and roles in cancer, ChemBioChem 18 (2017) 1146–1154, https://doi.org/10.1002/cbic.201600705.
[2] S. Sipione, J. Monyror, D. Galleguillos, N. Steinberg, V. Kadam, Gangliosides in the brain: physiology, pathophysiology and therapeutic applications, Front. Neurosci. 14 (2020) 572965, https://doi.org/10.3389/fnins.2020.572965.
[3] K. Wallom, M. Fernández-Suárez, D. Priestman, D. Vruchte, M. Huebecker, P. Hallett, O. Isacson, F. Platt, Glycosphingolipid metabolism and its role in ageing and Parkinson's disease, Glycoconj. J. 39 (2022) 39–53, https://doi.org/10.1007/s10719-021-10023-x.
[4] X. Jin, G.-Y. Yang, Pathophysiological roles and applications of glycosphingolipids in the diagnosis and treatment of cancer diseases, Prog. Lipid Res. 91 (2023) 101241, https://doi.org/10.1016/j.plipres.2023.101241.
[5] M.J. Sarmento, J.C. Ricardo, M. Amaro, R. Sachl, Organization of gangliosides into membrane domains, FEBS Lett. 594 (2020) 3668–3697, https://doi.org/10.1002/1873-3468.13871.
[6] R.L. Schnaar, Gangliosides of the vertebrate nervous system, J. Mol. Biol. 428 (2016) 3325–3336, https://doi.org/10.1016/j.jmb.2016.05.020.
[7] M.J. Sarmento, M.C. Owen, J.C. Ricardo, B. Chmelová, D. Davidovic, I. Mikhalyov, N. Gretskaya, M. Hof, M. Amaro, R. Vácha, R. Sachl, The impact of glycan headgroup on the nanoscopic segregation of gangliosides, Biophys. J. 120 (2021) 5530–5543, https://doi.org/10.1016/j.bpj.2021.11.017.
[8] M.G. Reis, R. Bibiloni, P. McJarrow, A. MacGibbon, B. Fong, S. Basset, N. Roy, M. M. Reis, Isotopic labeling of milk disialogangliosides (GD3), Chem. Phys. Lipids 200 (2016) 104–112, https://doi.org/10.1016/j.chemphyslip.2016.08.003.
[9] F. Tang, J. Wang, Y. Itokazu, R. Yu, Ganglioside GD3 regulates dendritic growth in newborn neurons in adult mouse hippocampus via modulation of mitochondrial dynamics, J. Neurochem. 156 (2021) 819–833, https://doi.org/10.1111/jnc.15137.
[10] M. Sorice, T. Garofalo, R. Misasi, V. Manganelli, R. Vona, W. Malorni, Ganglioside GD3 as a raft component in cell death regulation, Anti Cancer Agents Med. Chem. 12 (2012) 376–382, https://doi.org/10.2174/187152012800228670.
[11] D. Wu, N. Segal, S. Sidobre, M. Kronenberg, P. Chapman, Cross-presentation of Disialoganglioside GD3 to natural killer T cells, J. Exp. Med. 198 (2003) 173–181, https://doi.org/10.1084/jem.20030446.
[12] J. Park, D. Wu, M. Prendes, S. Lu, G. Ragupathi, N. Schrantz, P. Chapman, Fine specificity of natural killer T cells against GD3 ganglioside and identification of GM3 as an inhibitory natural killer T-cell ligand, Immunology 123 (1) (2008) 145–155, https://doi.org/10.1111/j.1365-2567.2007.02760.x.
[13] W. Tong, M. Maira, R. Roychoudhury, I. Pirvulescu, S. Moffett, H. Saragovi, Vaccination with tumor-ganglioside Glycomimetics activates a selective immunity that affords Cancer therapy, Cell Chem. Biol. 26 (2019) 1013–1026, https://doi.org/10.1016/j.chembiol.2019.03.018.
[14] J.N. Silva, A.C.N. Oliveira, M.P.P.A. Casal, A.C. Gomes, P.J. Coutinho, O. P. Coutinho, M.R. Oliveira, DODAB: monoolein-based lipoplexes as non-viral vectors for transfection of mammalian cells, Biochim. Biophys. Acta Biomembr. 1808 (2011) 2440–2449, https://doi.org/10.1016/j.bbamem.2011.07.002.
[15] T.R. Oliveira, C.R. Benatti, M.T. Lamy, Structural characterization of the interaction of the polyene antibiotic amphotericin B with DODAB bicelles and vesicles, Biochim. Biophys. Acta Biomembr. 1808 (2011) 2629–2637, https://doi.org/10.1016/j.bbamem.2011.07.042.
[16] J.H.K. Rozenfeld, S.R. Silva, P.A. Ranéia, E. Faquim-Mauro, A.M. Carmona-Ribeiro, Stable assemblies of cationic bilayer fragments and CpG oligonucleotide with enhanced immunoadjuvant activity in vivo, J. Control. Release 160 (2012) 367–373, https://doi.org/10.1016/j.jconrel.2011.10.017.
[17] L.R.M.M. Aps, M.B. Tavares, J.H.K. Rozenfeld, M.T. Lamy, L.C.S. Ferreira, M. O. Diniz, Bacterial spores as particulate carriers for gene gun delivery of plasmid DNA, J. Biotechnol. 228 (2016) 58–66, https://doi.org/10.1016/j.jbiotec.2016.04.027.
[18] G.K. Pedersen, P. Andersen, D. Christensen, Immunocorrelates of CAF family adjuvants, Semin. Immunol. 39 (2018) 4–13, https://doi.org/10.1016/j.smim.2018.10.003.
[19] D. Davidovic, M. Kukulka, M.J. Sarmento, I. Mikhalyov, N. Gretskaya, J. C. Chmelová Ricardo, M. Hof, L. Cwiklik, R. Sachl, Which moiety drives gangliosides to form nanodomains? J. Phys. Chem. Lett. 14 (2023) 5791–5797, https://doi.org/10.1021/acs.jpclett.3c00761.
[20] H. Heerklotz, The microcalorimetry of lipid membranes, J. Phys. Condens. Matter 16 (2004) R441–R467, https://doi.org/10.1088/0953-8984/16/15/R01.
[21] W.K. Subczynski, J. Widomska, J.B. Feix, Physical properties of lipid bilayers from EPR spin labeling and their influence on chemical reactions in a membrane environment, Free Radic. Biol. Med. 46 (2009) 707–718, https://doi.org/10.1016/j.freeradbiomed.2008.11.024.
[22] A. Catte, G.F. White, M.R. Wilson, V. Oganesyan, Direct prediction of EPR spectra from lipid bilayers: understanding structure and dynamics in biological membranes, ChemPhysChem 19 (2018) 2183–2193, https://doi.org/10.1002/cphc.201800386.
[23] J.H.K. Rozenfeld, E.L. Duarte, T.R. Oliveira, M.T. Lamy, Structural insights on biologically relevant cationic membranes by ESR spectroscopy, Biophys. Rev. 9 (2017) 633–647, https://doi.org/10.1007/s12551-017-0304-4.
[24] J.T. Mason, Investigation of phase transitions in bilayer membranes, Methods Enzymol. 295 (1998) 468–494, https://doi.org/10.1016/s0076-6879(98)95054-6.
[25] J.M. Boggs, G. Rangaraj, Phase transitions and fatty acid spin label behavior in interdigitated lipid phases induced by glycerol and polymyxin, Biochim. Biophys.

Acta Biomembr. 816 (1985) 221–233, https://doi.org/10.1016/0005-2736(85)90489-4.
[26] W.L. Hubbell, H.M. McConnell, Molecular motion in spin-labeled phospholipids and membranes, J. Am. Chem. Soc. 93 (1971) 314–326, https://doi.org/10.1021/ja00731a005.
[27] F.M. Linseisen, S. Bayerl, T.M. Bayerl, 2H-NMR and DSC study of DPPC-DODAB mixtures, Chem. Phys. Lipids 83 (1996) 9–23, https://doi.org/10.1016/0009-3084(96)02572-8.
[28] J.H. Rozenfeld, E.L. Duarte, L.R. Barbosa, M.T. Lamy, The effect of an oligonucleotide on the structure of cationic DODAB vesicles, Phys. Chem. Chem. Phys. 17 (2015) 7498–7506, https://doi.org/10.1039/C4CP05652C.
[29] J. Cocquyt, U. Olsson, G. Olofsson, P. Van der Meeren, Thermal transitions of DODAB vesicular dispersions, Colloid Polym. Sci. 283 (2005) 1376–1381, https://doi.org/10.1007/s00396-005-1347-9.
[30] P. Saveyn, P. Van der Meeren, M. Zackrisson, T. Narayanan, U. Olsson, Subgel transition in diluted vesicular dispersions, Soft Matter 5 (2009) 1735–1742, https://doi.org/10.1039/B821387A.
[31] F.G. Wu, Z.W. Yu, G. Ji, Formation and transformation of the subgel phase in dioctadecyldimethylammonium bromide aqueous dispersions, Langmuir 27 (2011) 2349–2356, https://doi.org/10.1021/la1049474.
[32] L. Andrade, E.L. Duarte, M.T. Lamy, J.H.K. Rozenfeld, Thermotropic behavior and structural organization of C24:1 sulfatide dispersions and its mixtures with cationic bilayers, ACS Omega 8 (2023) 5306–5315, https://doi.org/10.1021/acsomega.2c06189.
[33] A.G. Lee, Lipid phase transitions and phase diagrams I. Lipid phase transitions, Biochim. Biophys. Acta Rev. Biomembr. 472 (1977) 237–281, https://doi.org/10.1016/0304-4157(77)90018-1.
[34] L.S. Martins, E.L. Duarte, M.T. Lamy, J.H.K. Rozenfeld, Supramolecular organization of α-galactosylceramide in pure dispersions and in cationic DODAB bilayers, Chem. Phys. Lipids 232 (2020) 104963, https://doi.org/10.1016/j.chemphyslip.2020.104963.
[35] C.R. Benatti, E. Feitosa, R.M. Fernandez, M.T. Lamy-Freund, Structural and thermal characterization of dioctadecyldimethylammonium bromide dispersions by spin labels, Chem. Phys. Lipids 111 (2001) 93–104, https://doi.org/10.1016/S0009-3084(01)00134-7.
[36] H. Schindler, J. Seelig, EPR spectra of spin labels in lipid bilayers, J. Chem. Phys. 59 (1973) 1841–1850, https://doi.org/10.1063/1.1680269.
[37] A. Lange, D. Marsh, K.H. Wassmer, P. Meier, G. Kothe, Electron spin resonance study of phospholipid membranes employing a comprehensive line-shape model, Biochemistry 24 (1985) 4383–4392, https://doi.org/10.1021/bi00337a020.
[38] L.S. Martins, E.L. Duarte, M.T. Lamy, J.H.K. Rozenfeld, DODAB vesicles containing lysophosphatidylcholines: the relevance of acyl chain saturation on the membrane structure and thermal properties, Biophys. Chem. 300 (2023) 107075, https://doi.org/10.1016/j.bpc.2023.107075.
[39] J.B. Ejarque, E.L. Duarte, M.T. Lamy, J.H.K. Rozenfeld, Evidence for Ca^{2+}-induced structural change in diluted GD3 ganglioside dispersions, Biochim. Biophys. Acta Biomembr. 1866 (2024) 184271, https://doi.org/10.1016/j.bbamem.2024.184271.
[40] B. Maggio, T. Ariga, R.O. Calderóm, R.K. Yu, Ganglioside GD3 and GD3-lactone mediated regulation of the intermolecular organization in mixed monolayers with dipalmitoylphosphatidylcholine, Chem. Phys. Lipids 90 (1997) 1–10, https://doi.org/10.1016/S0009-3084(97)00090-X.
[41] E.J. Dufourc, Bicelles and nanodiscs for biophysical chemistry, Biochim. Biophys. Acta Biomembr. 1863 (2021) 183478, https://doi.org/10.1016/j.bbamem.2020.183478.
[42] I. Alahmadi, Jr D. Hoy, A.T. Rad, S. Patil, A. Alahmadi, J. Kinnun, H.L. Scott, J. Katsaras, M.P. Nieh, Changes experienced by low-concentration lipid bicelles as a function of temperature, Langmuir 38 (2022) 4332–4340, https://doi.org/10.1021/acs.langmuir.2c00078.
[43] V.K. Sharma, H. Srinivasan, V.G. Sakai, S. Mitra, Dioctadecyldimethylammonium bromide, a surfactant model for the cell membrane: importance of microscopic dynamics, Struct. Dyn. 7 (2020) 051301, https://doi.org/10.1063/4.0000030.
[44] L.S. Martins, D.A. Nomura, E.L. Duarte, K.A. Riske, M.T. Lamy, J.H.K. Rozenfeld, Structural characterization of cationic DODAB bilayers containing C24:1 β-glucosylceramide, Biochim. Biophys. Acta Biomembr. 1861 (2019) 643–650, https://doi.org/10.1016/j.bbamem.2018.12.018.
[45] H.L. Brockman, M.M. Momsen, R.E. Brown, L. He, J. Chun, H.S. Byun, R. Bittman, The 4, 5-double bond of ceramide regulates its dipole potential, elastic properties, and packing behavior, Biophys. J. 87 (2004) 1722–1731, https://doi.org/10.1529/biophysj.104.044529.
[46] I. Pascher, Molecular arrangements in sphingolipids conformation and hydrogen bonding of ceramide and their implication on membrane stability and permeability, Biochim. Biophys. Acta Biomembr. 455 (1976) 433–451, https://doi.org/10.1016/0005-2736(76)90316-3.
[47] S.L. Frey, E.Y. Chi, C. Arratia, J. Majewski, K. Kjaer, K.Y.C. Lee, Condensing and fluidizing effects of ganglioside GM1 on phospholipids films, Biophys. J. 94 (2008) 3047–3064, https://doi.org/10.1529/biophysj.107.119990.
[48] L. Cantù, E.D. Favero, S. Sonnino, A. Prinetti, Gangliosides and the multiscale modulation of membrane structure, Chem. Phys. Lipids 164 (2011) 796–810, https://doi.org/10.1016/j.chemphyslip.2011.09.005.
[49] M. Diociaiuti, I. Ruspantini, C. Giordani, F. Bordi, P. Chistolini, Distribution of GD3 in DPPC monolayers: a thermodynamic and atomic force microscopy combined study, Biophys. J. 86 (2004) 321–328, https://doi.org/10.1016/S0006-3495(04)74107-7.
[50] M.R. Bunow, B. Bunow, Phase behavior of ganglioside-lecithin mixtures. Relation to dispersion of gangliosides in membranes, Biophys. J. 27 (1979) 325–337, https://doi.org/10.1016/S0006-3495(79)85221-2.
[51] Grauby-Heywang C., Behavior of GM3 ganglioside in lipid monolayers mimicking rafts or fluid phase in membranes. Chem. Phys. Lipids 139: 68–76. DOI: https://doi.org/10.1016/j.chemphyslip.2005.10.003.
[52] E.H. Mojumdar, C. Grey, E. Sparr, Self-assembly in ganglioside-phospholipid systems: the co-existence of vesicles, micelles and disks, Int. J. Mol. Sci. 21 (2019) 56, https://doi.org/10.3390/ijms21010056.
[53] S. Sonnino, A. Prinetti, L. Mauri, V. Chigorno, G. Tettamanti, Dynamic and structural properties of sphingolipids as driving forces for the formation of membrane domains, Chem. Rev. 106 (2006) 2111–2125, https://doi.org/10.1021/cr0100446.
[54] F.G. Wu, R.G. Wu, H.Y. Sun, Y.Z. Zheng, Z.W. Yu, Demixing and crystallization of DODAB in DPPC-DODAB binary mixtures, Phys. Chem. Chem. Phys. 16 (2014) 15307, https://doi.org/10.1039/C4CP01707B.
[55] F.G. Wu, N.N. Wang, Z.W. Yu, Nonsynchronous change in the head and tail of dioctadecyldimethylammonium bromide molecules during the liquid crystalline to coagel phase transformation process, Langmuir 25 (2009) 13394–13401, https://doi.org/10.1021/la901989j.
[56] F.G. Wu, N.N. Wang, L.F. Tao, Z.W. Yu, Acetonitrile induces nonsynchronous interdigitation and dehydration of dipalmitoylphosphatidylcholine bilayers, J. Phys. Chem. B 114 (2010) 12685–12691, https://doi.org/10.1021/jp104190z.
[57] M. Hegde, S. Girisa, B.S. Aswani, M.S. Alqahtani, M. Abbas, G. Sethi, A. B. Kunnumakkara, Harnessing the potential role of gangliosides in immunomodulation and cancer therapeutics, Life Sci. 351 (2024) 122786, https://doi.org/10.1016/j.lfs.2024.122786.
[58] K. Vermaelen, Vaccine strategies to improve anti-cancer cellular immune responses, Front. Immunol. 10 (2019) 8, https://doi.org/10.3389/fimmu.2019.00008.
[59] O.S. Kumru, S.B. Joshi, D.E. Smith, C.R. Middaugh, T. Prusik, D.B. Volkin, Vaccine instability in the cold chain: mechanisms, analysis and formulation strategies, Biologicals 42 (2014) 237–259, https://doi.org/10.1016/j.biologicals.2014.05.007.

Update

Biophysical Chemistry

Volume 327, Issue , December 2025, Page

DOI: https://doi.org/10.1016/j.bpc.2025.107513

Biophysical Chemistry 327 (2025) 107513

Contents lists available at ScienceDirect

Biophysical Chemistry

journal homepage: www.elsevier.com/locate/biophyschem

Corrigendum to "Effect of disialoganglioside GD3 on the subgel, gel and fluid phases of cationic DODAB vesicles" [biophysical chemistry 326 (2025) 107503]

Julia B. Ejarque [a,1], Anna C.F. Couto [a,1], Thábata Matos [a], Evandro L. Duarte [b], M. Teresa Lamy [b], Julio H.K. Rozenfeld [a,*]

[a] Departamento de Biofísica, Escola Paulista de Medicina, Universidade Federal de São Paulo, R. Botucatu 862, 04023-062 São Paulo, SP, Brazil
[b] Instituto de Física, Universidade de São Paulo, Rua do Matão 1371, 05508090 São Paulo, SP, Brazil

The following are the supplementary data related to this article.

Figure S1-Effect of 0.05 mM GD3 on the heating thermograms of 2 mM DODAB vesicles. Scan rates were 20 °C/h and 10 °C/h.

Fig. S2- EPR spectra of 5-PCSL and 16-PCSL embedded in 2 mM DODAB vesicles, with or without 0.1 mM GD3, at temperatures below the gel-fluid transition. The total spectra width is 100 G.

Figure S3- Visible aspect of the DODAB and DODAB + GD3 dispersions (above); and DLS size distributions (below). The mean hydrodynamic diameters (Dz), Polydispersity Index (PDI) and zeta-potential (ZP) values are also shown.

Supplementary Figs. 1, 2, and 3 were missing. They are shown with captions below.

Appendix A. Supplementary data

Supplementary data to this article can be found online at https://doi.org/10.1016/j.bpc.2025.107513.

DOI of original article: https://doi.org/10.1016/j.bpc.2025.107503.
* Corresponding author.
E-mail address: julio.rozenfeld@unifesp.br (J.H.K. Rozenfeld).
[1] These authors contributed equally to the work.

https://doi.org/10.1016/j.bpc.2025.107513

Available online 21 August 2025
0301-4622/© 2025 Elsevier B.V. All rights are reserved, including those for text and data mining, AI training, and similar technologies.